Effect of graphene size on the photocatalytic activity of TiO2/poly(3-hexylthiophene)/graphene composite films

Yuanqing Song, Florian Massuyeau, Long Jiang, Yi Dan, Philippe Le Rendu, Thien-Phap Nguyen

Effect of graphene size on the photocatalytic activity of TiO_2/poly(3-hexylthiophene)/graphene composite films

Y. Song[a,b], F. Massuyeau[a], L. Jiang[b], Y. Dan[b,*], P. Le Rendu[a], T.P. Nguyen[a,*]

[a] *Institut des Matériaux Jean Rouxel, 2 rue de la Houssinière, BP32229, 44322, Nantes, France*
[b] *State Key Laboratory of Polymer Materials Engineering of China, Polymer Research Institute, Sichuan University, Chengdu, 610065, PR China*

For improving the photocatalytic activity of titanium dioxide (TiO_2), the use of appropriate conjugated polymers such as poly(hexylthiophene) (P3HT) to form composites with TiO_2 can extend the absorption for the light harvesting. Such photocatalytic materials also have a high charge separation ability, which increases the photocatalytic reaction. Besides, to reduce the electron-hole recombination rates, which impact strongly the photocatalytic performance, graphene by its high electrical conductivity, can be incorporated to the P3HT/TiO_2 composites in order to improve the charge transport in the materials. However, the effects of the graphene size on the photocatalytic behavior of composites have not been much studied so far.

In this work, we have investigated P3HT/graphene composites and we examined the effect of the graphene size on the morphology and optical properties of the materials. Optical characterizations using, Raman, Infrared, absorption, steady and time resolved photoluminescence have been performed on composites synthesized with different graphene sizes (expressed by graphene weight per surface unit). It has been shown that their properties depend on the graphene concentration and also on its size. Based on these results and analyses, we studied the photocatalytic activities of TiO_2/P3HT/graphene composite films through the degradation processes of a rhodamine solution under visible light irradiation in the presence of the composites. Highest performance was provided by composite samples containing graphene of medium size (150 m^2/g). The improvement of photocatalytic activity of these composites is related to an increase in contact surface between graphene and polymer resulting in a better charge transfer between materials, enhancing thus their performance.

1. Introduction

In the field of environmental remediation, titanium dioxide (TiO_2) is the most popular photocatalytic materials. Despite the fact that its efficiency is limited due to the large bandgap value, TiO_2 is still playing a predominant role in many applications for organic pollutant degradation. Very often, the oxide is employed in nanoparticle form as an active photocatalyst in composites using conjugated polymers such as poly (hexylthiophene) or P3HT, poly(aniline) or PANI and poly(pyrrole) or PPy which provide a flexible host matrix for the oxide particle and also extend the light absorption to the visible range [1,2], resulting in an enhanced photocatalytic performance. Hybridization of TiO_2 with carbonaceous materials such as carbon black, carbon nanotubes and graphene have been also investigated for obtaining high photocatalytic efficiency [3]. Among the carbon based materials, graphene having two dimensional sheet structure, large surface and high electron mobility is particularly attractive for use in catalytic reactions with TiO_2. Moreover, graphene blended with P3HT is also known as an efficient absorber in organic solar cells in which the charge separation is favored as graphene usually acts as quencher of the fluorescence of the conjugated polymer [4].

From the above considerations, making composites by associating TiO_2, P3HT and graphene will allow high efficiency photocatalysts with an efficient photocatalytic activity provided by the oxide, a extended light absorption range due to the polymer and a high charge transport by the presence of graphene. However, the main issue of hybrid nanocomposites comes usually from their structure and morphology as often observed in hybrid materials used as absorbers in solar cells [5,6]. The performance of devices strongly depends on the structural and morphological characteristics of the composites since they impact on the physical processes (light harvesting and charge transfer) that govern the device operation. P3HT/TiO_2 and P3HT/graphene composites have been investigated as photocatalysts [7–10] and as absorbers in solar cells [11,12]. Incorporation of P3HT to TiO_2 [7] was found to expand the absorption of the oxide to the visible range and to strongly increase the conversion of methyl orange with high photocatalytic

* Corresponding authors.
E-mail addresses: danyichenweiwei@163.com (Y. Dan), Thien-Phap.nguyen@cnrs-imn.fr (T.P. Nguyen).

stability. Study of the charge transfer process in P3HT -TiO_2 composites [8] has showed that the process can operate in both direction, that is, polymer to oxide and oxide to polymer depending on the energy of the excitation light. On the other hand, composites made of P3HT and graphene oxide exhibit broad-band absorption and fast charge transfer rate between the polymer and the oxide. These interesting properties have been exploited for photocatalysis applications [9] and correlation between the optical properties and the photocatalytic of the composites has been demonstrated. It has been also proved that incorporation of graphene into P3HT/Ag3PO4 composite increases the specific surface area of and enhances the photocatalytic activity of Ag_3PO_4 [10]. Based on the previous study results, the photocatalytic process in P3HT/graphene composites can be described as follows. Under light irradiation, excitons are created in P3HT and diffuse to the contact with TiO_2 or graphene where they will be dissociated into electrons and holes. Electrons are transferred to the conduction band of TiO_2 and graphene and react with adsorbed oxygen of organic pollutants at the surface to yield O_2^-. At the same time, holes are transferred to the valence band of TiO_2 and react with adsorbed H_2O to yield OH^*. Both anions O_2^- and radicals OH^* can oxidize and degrade organic pollutants by converting them into CO_2 and H_2O. Accordingly, a highly performant composite needs an efficient charge transfer between the polymer and the inorganic component(s). This condition implies a large area contact between the polymer and the inorganic components (oxide nanoparticles and graphene platelets). Comparatively, the size of oxide nanoparticles is much smaller than that of graphene nanosheets and the contact surface between P3HT and graphene is predominant in P3HT/graphene/TiO_2 composites, that is, the interactions between P3HT and graphene are determinant for optical process and charge transfer mechanism in the composites. Indeed, the influence of the graphene oxide size on the optoelectronic properties of P3HT based composites has been previously investigated [13]. The results of this study showed that the interaction between graphene oxide and polymer depends on the size of the oxide nanoparticles and affects the optical properties of the composites.

As the size of the graphene platelets would influence the morphology and the structure of composite films, we studied the effect of graphene size in the composites made of P3HT and graphene nanoplatelets. Using optical spectroscopy including absorption, Infrared, Raman and steady state and time-resolved photoluminescence (PL) we analyzed the electronic structure of the composites as a function of the graphene concentration and size and examined the interactions between graphene and P3HT. From the obtained results, we discussed the possible transfer mechanisms occurring in the composites and to further support our hypotheses, we performed experiments to measure the photocatalytic activity of P3HT/TiO_2/graphene catalysts containing graphene platelets of different sizes.

2. Experimental

P3HT and graphene nanoplatelets (GNPs) were purchased from Rieke Metal and Nanovia. The molecular weight of P3HT (high regioregularity: > 98%) is 50 kDa given by the supplier. The graphene platelets are characterized by their surface per gramme and provided by the supplier. The size of the platelets is determined by measuring their average diameters. We used three different qualities of graphene nanoplatelets labeled G80 (of surface per gramme 60–80 m^2/g), G150 (of surface per gramme 120–150 m^2/g) and G750 (of surface per gramme 750 m^2/g) to consider the influence of the contact area of graphene in the conjugated polymer matrix. The P3HT/graphene nanoplatelets (P3HT/G80, P3HT/G150 and P3HT/G750) composites were prepared by the following procedure: 0.01 g P3HT solids were dissolved in 1.0 mL chlorobenzene. Different masses of graphene (0.0001, 0.0002, 0.0005, 0.0010, and 0.0020 g) were added to P3HT solutions. After continuously ultrasonicated at room temperature for 30 min, the mixture was utilized to deposit thin films on glass and KBr substrates by solvent-casting. The samples were dried under nitrogen flow and composite films of P3HT/G80, P3HT/G150 and P3HT/G750 were obtained with several of mass ratios (1:0.01, 1:0.02, 1:0.05, 1:0.10, and 1:0.20). P3HT/TiO_2/graphene composites with different sizes of graphene were prepared by the same method by adding 0.01 g TiO_2 powder to the P3HT/graphene solutions for achieving the following compositions (1:1:0.02, 1:1:0.05, 1:1:0.10, and 1:1:0.20). The composite films were then deposited by casting on appropriate substrates after sonication of the solution. The film thickness in the range of 0.1 to 1 μm was measured by a Dektak 8 Bruker profilometer. For a reliable comparison of results, samples having a same thickness were used for each experiment.

FT-IR measurements were carried out using a Bruker Vertex 70 FT-IR spectrometer in the range of 400–4000 cm^{-1} with 1 cm^{-1} resolution, using KBr as a reference sample. Raman spectra were recorded on a Renishaw InVia reflex spectrometer using an argon-ion laser source (λ = 514 nm) and UV–vis absorption spectra on a Varian Cary 5 G UV–vis-Nir spectrophotometer equipped with an integrating sphere. Scanning Electron Microscopy (SEM) analyses were performed with a field emission JEOL JSM-7600F microscope. PL measurements were performed using a Jobin-Yvon Fluorolog 3 spectrophotometer at room temperature, using a 400 nm excitation wavelength. Time-resolved PL experiments were carried out with a regenerative amplified femtosecond Ti:sapphire laser system (Spectra Physics Hurricane X) generating 100 fs pulses at 800 nm with a repetitive rate of 1 kHz and a power of 1 W. The laser line is frequency-doubled with a thin BBO crystal to obtain an excitation line λ_{exc} = 400 nm (3.1 eV) and the decayed fluorescence is detected at 700 nm. The transient signals were spectrally dispersed into a Princeton Instruments SP2300 imaging Acton spectrograph, and were temporally resolved with a high dynamic range Hamamatsu C7700 streak camera.

An aqueous solution of rhodamine B (RhB) was used as a model contaminant for studying the adsorption performance and photocatalytic activity of the composites. The films deposited on glass substrates containing 60 mg of photocatalyst were immersed in 200 mL RhB solution (10 mg/L). The solution and the films were then put into a 500 mL crystallizing dish. Before irradiation, the solution and the composites were kept in the dark for 40 min for obtaining desorption equilibrium of the system. A 500 W tungsten-halogen lamp wavelength range: 350–2500 nm), used as the visible light irradiation source, was positioned over the RhB solution to keep a constant irradiance of 70 mW/cm^2. A 420 nm filter was used to cut off the UV light below 420 nm.

The mixture was magnetically stirred throughout the experiments, and a portion of the samples was withdrawn at regular times. The change in the concentration of RhB was monitored by measuring the absorbance at λ_{max} = 553 nm with a UV-2300 UV–vis spectrophotometer (Hitachi) and the photocatalytic conversion (η) of RhB was calculated by:

$$\eta = \frac{A_0 - A_t}{A_0} \times 100 \quad (1)$$

where A_0 is the absorbance of initial RhB solution and A_t is its absorbance at time t.

3. Results and discussion

In order to understand the effect of the graphene size in photocatalytic process of the composites, it appears necessary to investigate first the properties of the different size graphene materials and their impact on the P3HT/graphene composite properties. The results can then be used to explain the photocatalytic performance of the active material composed of TiO_2, P3HT and graphene with different sizes.

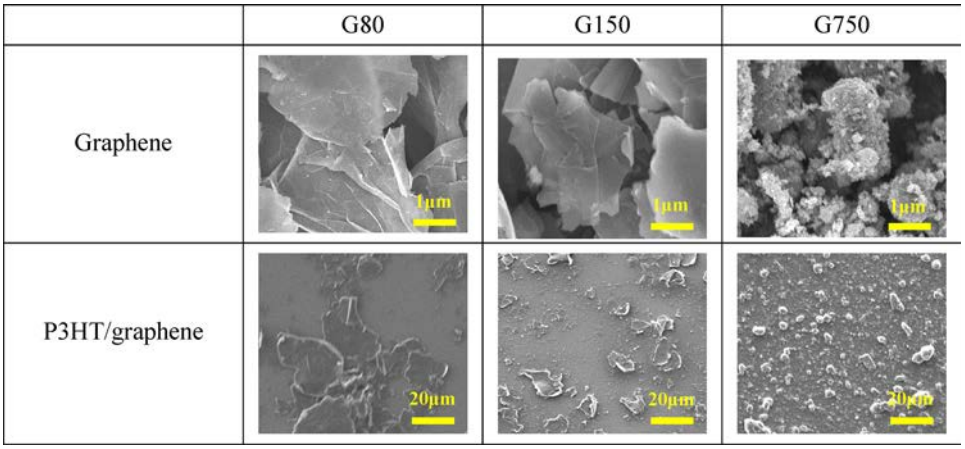

Fig. 1. SEM images of graphene and P3HT/ graphene composites.

3.1. SEM images and morphologies of samples

Fig. 1 shows the SEM images of different types of graphene and P3HT/graphene composites used in this study. The sizes of the graphene platelets are estimated to be 25, 15 and ≤ 2 μm for G80, G150 and G750 respectively. It can be seen that the morphology of graphene powders depends on their size. Large (G80) and medium size (G150) graphene platelets are thin sheets of different diameters while small size platelets seem to aggregate forming small clusters. As for composite samples, it can be observed that graphene is intimately incorporated into the polymer matrix. Large size graphene sheets (G80) tend to aggregate while small size graphene (G750) are more uniformly dispersed in the polymer films, due its small thickness and size. In the latter, clusters of platelets are observed as in G750 graphene powder. Medium graphene platelets G150 are thin sheets like G80 and are less well distributed in the polymer matrix than G750.

3.2. Raman spectroscopy

Fig. 2 shows Raman spectra of graphene and P3HT/graphene composite films. The typical bands of graphene are localized in the range 1343–1356 and 1568 - 1581 cm^{-1}, corresponding to D and G bands (Fig. 2a). These two bands reflect the level of disorder of graphene, and the intensity ratio I_D/I_G is indicative of the disorder degree of the material [14]. For G750 graphene, the I_D/I_G ratio equals 0.67 indicating a high disorder in the material.

The G band (E_{2g} mode) is common to all sp^2 carbon and provides information on the in-plane vibration of sp^2 bonded carbon atoms [15], while D band (A_{1g} mode) is assigned to the presence of sp^3 defects in graphite such as bond-angle disorder, bond-length disorder, vacancies, and edge defects [16]. The intensity of this band is strongest in G750 and decreases when the graphene size increases indicating that this material contain more defects than the large and medium size graphene. The presence of high concentration defects in small size graphene is in agreement with the SEM image and suggests that edge defects are dominant in this case. Furthermore, in the range 2685–2727 cm^{-1} the 2D band, also referred to the G' band, is observed. This band is the D band overtone and is always observed in graphite samples [15,16]. It has been established by theoretical calculations and by experiments that the G' band changes in shape and position with increasing number of graphene layers [17]. In Fig. 2, the peak position of the G' bands shifts from 2727 (in G80) to 2685 cm^{-1} (in G750). A red shift of this band is commonly associated with the reduction in the number of layers [18]. Therefore, the observed shift indicates that thinner layers of graphene are formed in small size graphene (G750), and this result is in full agreement with the structure and morphology of the material.

Fig. 2b shows the Raman spectra (measured at 514 nm) of P3HT, P3HT/G80, P3HT/G150 and P3HT/G750 composites. For pristine P3HT film, the strong intensity band localized at around 1449 cm^{-1} in the spectrum can be assigned to C=C stretching vibrations [19]. The band at 1378 cm^{-1} of smaller intensity corresponds to C–C stretching vibration of the macromolecular chains of P3HT [19]. Upon incorporation of graphene to P3HT, the Raman bands corresponding to the polymer have been unchanged, suggesting that graphene of different sizes did not impact on the vibrational modes of P3HT. This result differs from that obtained in graphene oxide nanoparticle/P3HT composites [13] in which the Raman bands of P3HT are modified upon incorporation of graphene. Indeed, the small sizes of particles (~50 nm) could break and decrease the conjugation length of the chain segments in the polymer, which leads to a shift of the Raman bands. In our composites, the graphene platelets have much larger size (> 2 μm)

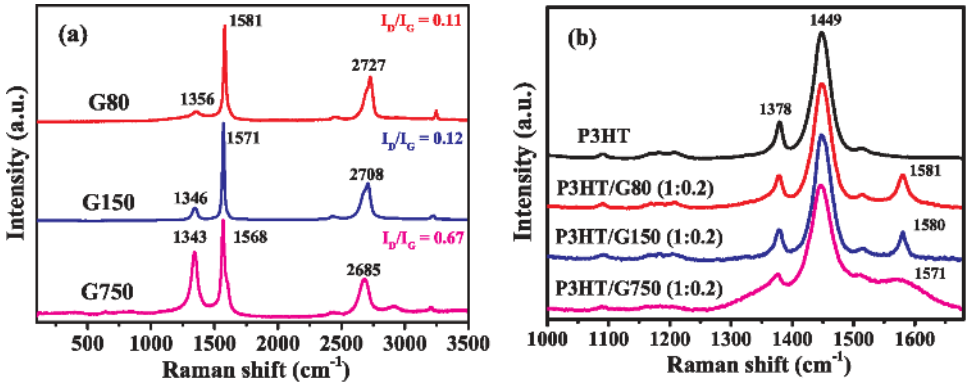

Fig. 2. Raman spectra of : a) G80, G150 and G750 graphene; b) P3HT, P3HT/G80, P3HT/G150 and P3HT/G750.

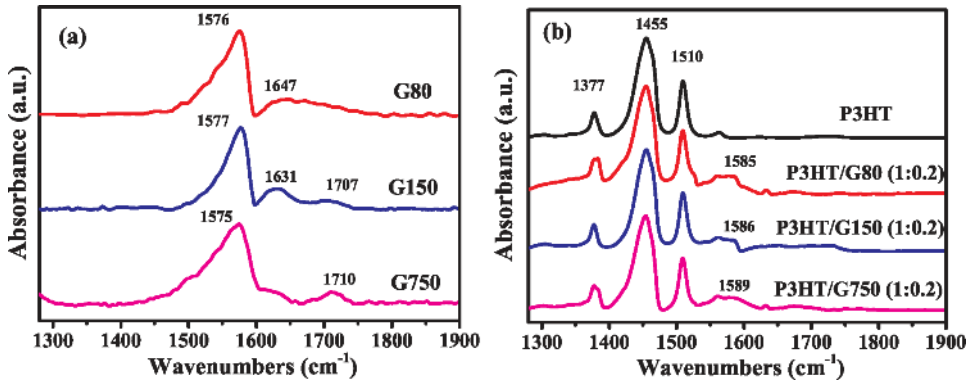

Fig. 3. Infra red spectra of : a) G80, G150 and G750 graphene; b) P3HT, P3HT/G80, P3HT/G150 and P3HT/G750 composites.

and the contact area between graphene and P3HT takes place on the surface of the platelets with no structural change of the polymer. In addition, only the G band of graphene could be observed with a slight red shift for small and medium size sheets. This could be explained by the large area contact of graphene with P3HT, which is an electron acceptor material [20]. It should be noted that in the P3HT/G750 sample, the G band is broadened and the D band intensity is increased (seen by a shoulder in the 1530 cm^{-1} region) as compared to the two other composites. The evolution of these bands can be seen as an increased disorder that is possibly due to oxidation of the material [13].

3.3. Infrared spectroscopy

The FT-IR spectra of graphene and P3HT/graphene composites are displayed in Fig. 3. For three types of graphene, the spectra show an absorption band at 1576 cm^{-1} assigned to the skeletal vibration C=C of graphene sheets (Fig. 3a). The absorption band at 1631 ~ 1647 cm^{-1} corresponds to O−H groups and the band at 1707 ~ 1723 cm^{-1} is assigned to C=O stretching vibrations from carbonyl and carboxylic groups [21]. It can be noted that the G750 graphene spectrum shows a strong carbonyl band compared with the two other spectra, indicating a possible oxidation of graphene at the film surface.

For the polymer, three characteristic bands are observed (Fig. 3b). The absorption band at 1377 cm^{-1} corresponds to CH_3 deformation, the band at 1455 cm^{-1} corresponds to symmetric C=C stretching mode of thiophene ring, and the band at 1510 cm^{-1} is assigned to the antisymmetric C=C stretching mode [22,23]. Incorporation of graphene to P3HT does not modify the vibrational bands of the polymer, confirming the Raman results. Note that an onset of the absorption band occurs at 1585 ~ 1589 cm^{-1}, which is assigned to the skeletal vibration of graphene sheets.

3.4. Absorption and photoluminescence spectroscopies

The photoemission arises from the recombination of photo-induced excitons or hole-electron pairs. Therefore, analysis of photoluminescence (PL) spectra can provide information for studying the creation, migration, and dissociation of excitons.

Fig. 4 shows UV–vis absorption spectra of P3HT, P3HT/G80, P3HT/G150 and P3HT/G750 composites. Threebands assigned to the 0-0, 0–1, 0-2 transitions can be retrieved, the absorption spectra of the samples being normalized to the maximum intensity of the 0-1 band. In accordance with the literature [13,20,24,25], the 0-0 band is associated with the recombination of excitons from intra-chain states while the 0-1 and 0-2 bands are attributed to the inter-chain states. Inspection of the spectra reveals an enhancement of the 0-0 transition peak and a decrease of the 0-2 peak after incorporation of graphene to pristine P3HT. These spectral modifications suggest a weakening of interchain interactions of the P3HT polymer chains due to embedding of the graphene

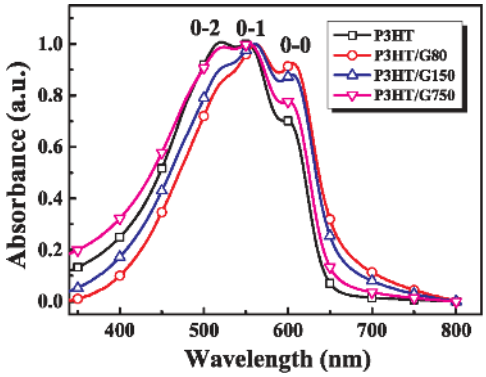

Fig. 4. UV–vis absorption spectra of P3HT, P3HT/G80, P3HT/G150 and P3HT/G750 composites.

sheets, implying the existence of a large hetero-interface in the P3HT/graphene composites. It should be noted in Fig. 4 that the variations of the 0-0 and 0-2 transitions are strongly correlated for all the graphene sizes used for composites, i.e., the highest increase in 0-0 transitions corresponds to the strongest decrease of 0-2 transitions (in P3HT/G80). This implies that the formation of J-aggregates takes place in these composites to the detriment of H-aggregates and vice versa.

For investigation of energy and charge transfer mechanisms between P3HT and graphene, steady-state and time–resolved photoluminescence experiments have been carried out [26–28]. First, the PL emission spectra of P3HT/G80, P3HT/G150 and P3HT/G750 composites with different graphene concentrations are shown in Fig. 5. The intensity of P3HT/G80, P3HT/G150 and P3HT/G750 spectra are significantly reduced as compared to that of the pristine polymer with increasing concentration of graphene, whatever their size. This result suggests that incorporation of graphene sheets to the polymer leads to quenching of its fluorescence. To illustrate the decrease in fluorescence of P3HT, we plot in Fig. 6 the ratio of the 0-1 transition intensity I^{0-1}/I_0^{0-1} as a function of the graphene concentration for three graphene sizes. I_0^{0-1} is the 0-1 transition intensity of pristine P3HT. It can be seen that the decrease in fluorescence reaches ~ 80–90% of the initial emission, indicating that the dissociation of excitons occurs in composites and increases with the graphene concentration. This result obviously gives prominence to the interface between graphene and P3HT in the charge dissociation process. We notice however that contrary to what can be expected, the exciton quenching is less important in small graphene size (G750) based composite samples. This behavior may be explained by the grain-like shape of the G750 graphene, which offer a smaller contact area with the polymer films while G150 and G80 graphene platelets are composed of thin and larger surface sheets, therefore offer more contact area to P3HT. Another possible cause of this charge dissociation difference may be the consequence of the uniform

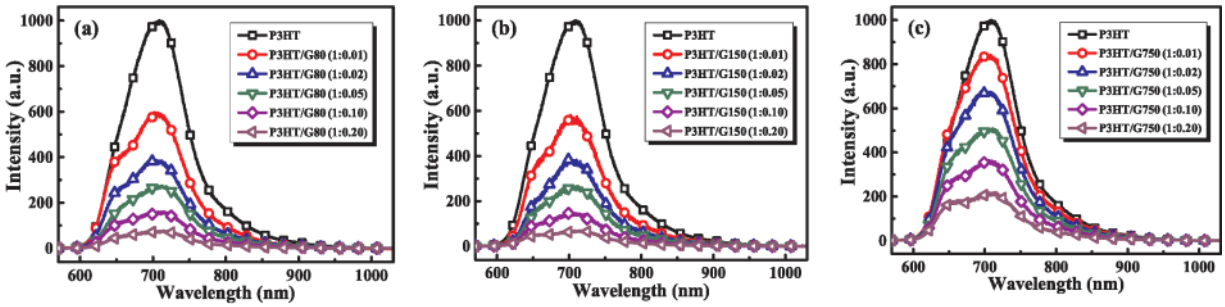

Fig. 5. Photoluminescence emission spectra of : (a) P3HT/G80, (b) P3HT/G150 and (c) P3HT/G750 composites with different graphene concentrations.

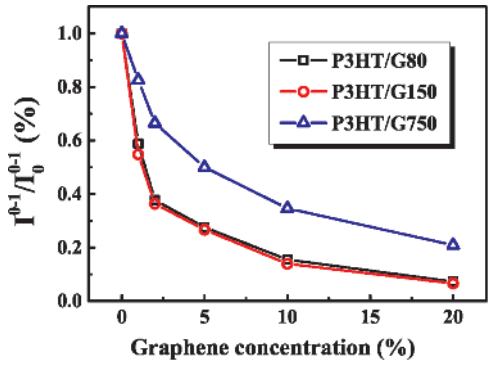

Fig. 6. Photoluminescence intensity ratios I^{0-1}/I_0^{0-1} of P3HT/G80, P3HT/G150, P3HT/G750 composites as a function of graphene concentration.

dispersion of G750 graphene on the surface of the composite film. Indeed, this distribution favors the charge dissociation on the surface of the films but is unfavorable to that in the film volume. On the contrary, in both G80 and G150 based composites, the graphene platelets on the surface and in the polymer bulk can achieve charge dissociation due to their different morphology.

To further investigate the mechanism of charge transfer between P3HT and graphene, time resolved photoluminescence experiments have been performed on P3HT and its composites. The normalized photoemission decay curves are given in Fig. 7. The photoluminescence decays can be described by two lifetimes τ_1 and τ_2 and the PL intensity curves can be plotted using the following equation: $I(t) = I_0 + A_1 e^{-\frac{t}{\tau 1}} + A_2 e^{-\frac{t}{\tau 2}}$. The average decay time is then determined using the expression: $\tau_a = \langle \tau \rangle = \sum_i A_i \tau_i$ and is displayed on Fig. 7 for P3HT and its composites.

The average decay time of P3HT/G80, P3HT/G150 and P3HT/G750 composites are significantly reduced as compared to that of the pure polymer (228 ps). The shortened lifetime of P3HT afteraddition of graphene to the polymer is obviously a consequence of electron transfer process from the photo-excited P3HT chains to graphene sheets [29]. The most efficient transfer is observed in P3HT/G150 composites (average decay time of 114 ps) and the result is consistent with that obtained in PL emission experiment. Indeed, the weak charge transfer rate observed in composites using G750 graphene may be assigned to the high defect concentration in graphene as detected by Raman spectroscopy. G80 and G150 based composites contain less defect, which can explain their lower average decay. Moreover, from SEM analysis, graphene platelets in G150 composites seem to be better distributed in P3HT and are thinner than those of G80. Consequently, the graphene/polymer interface in G150 composites has a larger area and the distance between graphene platelets is reduced, leading to a high exciton concentration with a short diffusion length therefore a high charge transfer.

3.5. Analysis on the photocatalytic activity

From the material analysis results, the size of graphene platelets impacts on P3HT/graphene composite optical properties and expectedly, on their photocatalytic behavior. To check this possible correlation, we fabricated composites using TiO_2 anatase as a photocatalyst associated with P3HT/graphene composites in order to improve the light absorption and the charge transport. To test the charge transfer hypothesis in photocatalysis, we used different graphene sizes for a given composition of TiO_2/P3HT/graphene composites and we compared their performance in degradation experiments of rhodamine B (RhB). The conversion of RhB is due to the breaking of bondings in the chromophoric groups by photocatalytic oxidation.

Prior to the photocatalytic experiments, the adsorption behaviors of the samples were studied by measuring the RhB adsorption efficiency as a function of time. In Fig. 8, the variation of the RhB adsorption ratio in

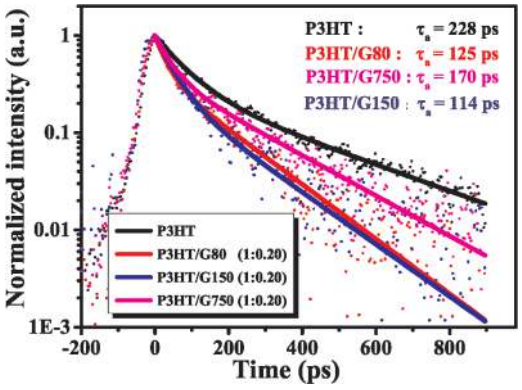

Fig. 7. Time-resolved photoluminescence decay profiles of P3HT and P3HT/graphene (1 : 0.20) composite films with various graphene sizes. The average decay time τ_a is calculated for all the materials using the technique described in the text.

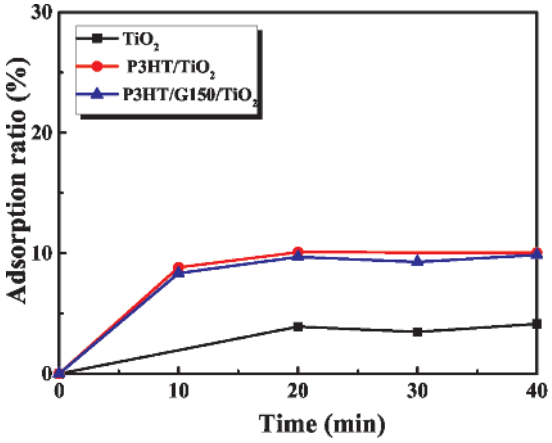

Fig. 8. Variation of adsorption ratio of RhB as a function of time under dark using TiO_2, P3HT/TiO_2 (1 : 2), and P3HT/G150/TiO_2 (1 : 0.2 : 2) composites.

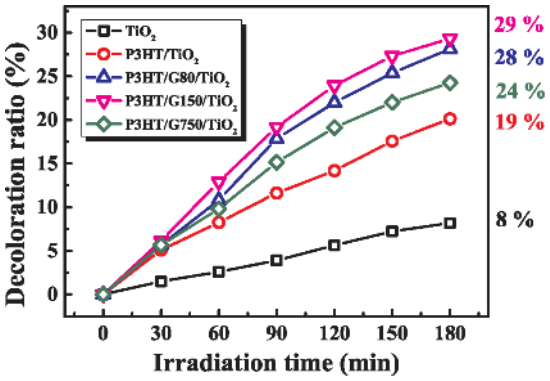

Fig. 9. Variation of decoloration ratio of RhB as a function of irradiation time under visible light by using TiO_2, P3HT/TiO_2 (1 : 2), P3HT/G80/TiO_2 (1 : 0.2 : 2), P3HT/G150/TiO_2 (1 : 0.2 : 2) and P3HT/G750/TiO_2 (1 : 0.2 : 2) composites. The decoloration ratio measured after 3 h of exposure is displayed for each photocatalyst on the right side of the figure.

presence of TiO2 and composites of P3HT/TiO_2, P3HT/G150/$TiO_2$is shown. It can be seen that a weak adsorption of RhB occurs with added TiO_2, which increases when P3HT and graphene are further incorporated. After 40 min of desorption equilibrium, the adsorption ratio reached ~4% for TiO_2 and ~10% for the composites and did not show any further evolution afterwards.

Fig. 9 shows the photocatalytic conversion of RhB as a function of time, the composite films being exposed to visible light in presence of the dye. TiO_2 and four composites including P3HT/TiO_2, P3HT/G80/TiO_2, P3HT/G150/TiO_2 and P3HT/G750/TiO_2 have been measured Compared to the bare TiO_2 oxide, the photocatalytic performance of P3HT/TiO_2 composites is better (a conversion of 19% compared to 9% after 3 h of exposure) because of the extension of light absorption to the visible range, which enhances the number of created excitons in the materials. Upon incorporation of graphene the performance is again improved (a conversion higher than 24% for 3 h of exposure) because of a better charge transport induced by graphene platelets. We notice that the conversion of P3HT/graphene/TiO_2 composites depends on the graphene platelet size, and the highest photocatalytic activity is obtained in P3HT/G150/TiO_2 samples. We explain this result by considering the properties of the composites studied previously. The medium size of graphene favors a relatively uniform dispersion of the platelets in the polymer matrix both on the surface and in the volume. These platelets by their size allow the creation of excitons on the surface and in the volume of the composite film. Another consequence of the graphene size is the short diffusion length of excitons producing an efficient quenching and charge separation. Finally, the rather low defect concentration in the G150 graphene provides an efficient charge transport and charge transfer to the composites and consequently a higher rate of pollutant degradation.

4. Conclusion

In this paper, we have fabricated composites made of P3HT and graphene of different sizes and concentrations and studied their properties by optical spectroscopy and microscopy. For a given graphene concentration, the morphology of the composite films is found to be dependent on the size of graphene with a grain-like shape for small graphene platelets and sheet-like shape for larger size ones. The incorporation of graphene in the polymer films impacts on the charge separation process during exposure to visible light. The size of graphene platelets has a strong influence on the charge transfer between the polymer and graphene. Using P3HT/graphene composites with TiO_2 nanoparticles as a photocatalyst, we measured the degradation of RhB and compared the photocatalytic performance of composites with different sizes of graphene platelets. The best efficiency was obtained with a medium size graphene (G150) composites, and the results are explained by a film morphology favorable to light absorption and a structure facilitating the charge transfer between graphene and polymer.

Acknowledgements

The authors are grateful to the National Natural Science Foundation of China (Grants: 50573052, 51173116, and 51573109) for supporting this research. We gratefully acknowledge China Scholarship Council (CSC) and Campus France for providing financial support for a cotutelle thesis and France-China scientific collaboration project.

References

[1] K.R. Reddy, M. Hassan, V.G. Gomes, Hybrid nanostructures based on titanium dioxide for enhanced photocatalysis, Appl. Catal. A Gen. 489 (2015) 1–16.
[2] J. Park, Visible and near infrared light active photocatalysis based on conjugated polymers, Ind. Eng. Chem. Res. 51 (2017) 27–43.
[3] F. Petronella, A. Truppi, C. Ingrosso, T. Placido, M. Striccoli, M.L. Curri, A. Agostiano, R. Comparelli, Nanocomposite materials for photocatalytic degradation of pollutants, Catal. Today 281 (2017) 85–100.
[4] C.M. Hill, Y. Zhu, S. Pan, Fluorescence and electroluminescence quenching evidence of interfacial charge transfer in poly(3-hexylthiophene): graphene oxide bulk heterojunction photovoltaic devices, ACS Nano 5 (2011) 942–951.
[5] W.U. Huynh, J.J. Dittmer, W.C. Libby, G.L. Whiting, A.P. Alivisatos, Controlling the morphology of nanocrystal-polymer composites for solar cells, Adv. Funct. Mater. 13 (2003) 73–79.
[6] M. Wright, A. Uddin, Organic-inorganic hybrid solar cells: a comparative review, Sol. Energy Mater. Sol. Cells 107 (2012) 87–111.
[7] D. Wang, J. Zhang, Q. Luo, X. Li, Y. Duan, J. An, Characterization and photocatalytic activity of poly(3-hexylthiophene)-modified TiO_2 for degradation of methyl orange under visible light, J. Hazard. Mater. 169 (2009) 546–550.
[8] L. Jiang, J. Zhang, W. Wang, H. Yang, F. Reisdorffer, T.P. Nguyen, Y. Dan, Optical properties of poly(3-hexylthiophene) and interfacial charge transfer between poly (3-hexylthiophene) and titanium dioxide in composites, J. Lumin. 159 (2015) 88–92.
[9] S. Wang, C.T. Nai, X.F. Jiang, Y. Pan, C.H. Tan, M. Nesladek, Q.H. Xu, K.P. Loh, Graphene oxide-polythiophene hybrid with broad-band absorption and photocatalytic properties, J. Phys. Chem. Lett. 3 (2012) 2332–2336.
[10] Y. Zhang, C. Xie, F.L. Gu, H. Wu, Q. Guo, Significant visible-light photocatalytic enhancement in rhodamine B degradation of silver orthophosphate via the hybridization of N-doped graphene and poly(3-hexylthiophene), J. Hazard. Mater. 315 (2016) 23–34.
[11] C.Y. Kwong, W.C.H. Choy, A.B. Djurisic, P.C. Chui, K. WCheng, W.K. Chan, Poly(3 hexylthiophene):TiO_2 nanocomposites for solar cell applications, Nanotechnology 15 (2004) 1156–1161.
[12] Q. Liu, Z. Liu, X. Zhang, L. Yang, N. Zhang, G. Pan, S. Yin, Y. Chen, J. Wei, Polymer photovoltaic cells based on solution-processable graphene and P3HT, Adv. Funct. Mater. 19 (2009) 894–904.
[13] P. Sriram, R. Nutenki, V.R. Mandapati, M. Karuppiah, S.I. Kattimuttathu, Effect of graphene oxide size and structure on synthesis and optoelectronic properties of hybrid graphene oxide-poly (3-hexylthiophene) nanocomposites, Polym. Comp. 38 (2017) 852–862.
[14] A.J. Pollard, B. Brennan, H. Stec, B.J. Tyler, M.P. Seah, I.S. Gilmore, D. Roy, Quantitative characterization of defect size in graphene using Raman spectroscopy, App. Phys. Lett. 106 (2014) 253107.
[15] F. Tuinstra, J.L. Koenig, Raman spectrum of graphite, J. Chem. Phys. 53 (1970) 1126–1130.
[16] R.P. Vidano, D.B. Fischbach, L.J. Willis, T.M. Loehr, Observation of Raman band shifting with excitation wavelength for carbons and graphites, Solid State Commun. 39 (1981) 341–344.
[17] A.C. Ferrari, J.C. Meyer, V. Scardaci, C. Casiraghi, M. Lazzeri, F. Mauri, S. Piscanec, D. Jiang, K.S. Novoselov, S. Roth, A.K. Geim, Raman spectrum of graphene and graphene layers, Phys. Rev. Lett. 97 (2006) 187401.
[18] L.M. Malard, M.A. Pimenta, G. Dresselhaus, M.S. Dresselhaus, Raman spectroscopy in graphene, Phys. Rep. 473 (2009) 51–87.
[19] N.J. Alley, K.S. Liao, E. Andreoli, S. Dias, E.P. Dillon, A.W. Orbaek, A.R. Barron, H.J. Byrne, S.A. Curran, Effect of carbon nanotube-fullerene hybrid additive on P3HT:PCBM bulk-heterojunction organic photovoltaics, Synth. Met. 162 (2012) 95–101.
[20] V.Z. Poenitzsch, D.C. Winters, H. Xie, G.R. Dieckmann, A.B. Dalton, I.H. Musselman, Effect of electron-donating and electron-withdrawing groups on peptide / single-walled carbon nanotube interactions, J. Am. Chem. Soc. 129 (2007) 14724–14732.
[21] M. Beidaghi, C.L. Wang, Micro-Supercapacitors based on interdigital electrodes of reduced graphene oxide and carbon nanotube composites with ultrahigh power handling performance, Adv. Funct. Mater. 22 (2012) 4501–4510.
[22] R. Koizhaiganova, H.J. Kim, T. Vasudevan, S. Kudaibergenov, M.S. Lee, In situ polymerization of 3-Hexylthiophene with double-walled carbon nanotubes: studies on the conductive nanocomposite, J. Appl. Polym. Sci. 115 (2010) 2448–2454.

[23] V. Saini, O. Abdulrazzaq, S. Bourdo, E. Dervishi, A. Petre, V.G. Bairi, T. Mustafa, L. Schnackenberg, T. Viswanathan, A.S. Biris, Structural and optoelectronic properties of P3HT-graphene composites prepared by in situ oxidative polymerization, J. Appl. Phys. 112 (2012) 054327.
[24] P.J. Brown, D.S. Thomas, A. Köhler, J.S. Wilson, J.S. Kim, C.M. Ramsdale, H. Sirringhaus, R.H. Friend, Effect of interchain interactions on the absorption and emission of poly3-hexylthiophene, Phys. Rev. B 67 (2003) 064203.
[25] E.T. Niles, J.D. Roehling, H. Yamagata, A.J. Wise, F.C. Spano, A.J. Moulé, J.K. Grey, J-Aggregate behavior in Poly-3-hexylthiophene nanofibers, J. Phys. Chem. Lett. 3 (2012) 259–263.
[26] S. Wang, C.T. Nai, X.F. Jiang, Y. Pan, C.H. Tan, M. Nesladek, Q.H. Xu, K.P. Loh, Graphene oxide – polythiophene hybrid with broad-band absorption and photocatalytic properties, J. Phys. Chem. Lett. 3 (2012) 2332–2336.
[27] F. Zheng, W.L. Xu, H.D. Jin, X.T. Hao, K.P. Ghiggino, Charge transfer from poly(3-hexylthiophene) to graphene oxide and reduced graphene oxide, RSC Adv. 5 (2015) 89515–89520.
[28] Y. Wang, D. Kurunthu, G.W. Scott, C.J. Bardeen, Fluorescence quenching in conjugated polymers blended with reduced graphitic oxide, J. Phys. Chem. C 114 (2010) 4153–4159.
[29] C. Ran, M. Wang, W. Gao, Jijun Ding, Y. Shi, X. Song, H. Chen, Z. Ren, Study on photoluminescence quenching and photostability enhancement of MEH-PPV by reduced graphene oxide, J. Phys. Chem. C 116 (2012) 23053–23060.